Microscopic theory of the optical properties of colloidal graphene quantum dots

Isil Ozfidan,[1,2] Marek Korkusinski,[1] A. Devrim Güçlü,[3] John A. McGuire,[4] and Pawel Hawrylak[1,2]

[1]*Quantum Theory Group, Security and Disruptive Technologies, Emerging Technologies Division, National Research Council of Canada, Ottawa, Canada K1A OR6*

[2]*Physics Department, University of Ottawa, Ottawa, Canada*

[3]*Department of Physics, Izmir Institute of Technology IZTECH, Izmir, Turkey*

[4]*Department of Physics and Astronomy, Michigan State University, East Lansing, Michigan 48824, USA*

(Received 28 October 2013; revised manuscript received 15 January 2014; published 21 February 2014)

We present a microscopic theory of electronic and optical properties of colloidal graphene quantum dots (CGQDs). The single-particle properties are described in the tight-binding model based on the p_z carbon orbitals. Electron-electron screened Coulomb direct, exchange, and scattering matrix elements are calculated using Slater p_z orbitals. The many-body ground state and excited states are constructed as a linear combination of a finite number of excitations from the Hartree-Fock (HF) ground state (GS) by exact diagonalization techniques. HF ground states corresponding to semiconductor, Mott-insulator, and spin-polarized phases are obtained as a function of the strength of the screened interaction versus the tunneling matrix element. In the semiconducting phase of a triangular CGQD, the top of the valence band and the bottom of the conduction band are found to be degenerate due to rotational symmetry. The singlet and triplet exciton spectra from the HF GS are obtained by solving the Bethe-Salpeter equation. The low-energy exciton spectrum is predicted to consist of two bright-singlet exciton states corresponding to two circular polarizations of light and a lower-energy band of two dark singlets and 12 dark triplets. The robustness of the bright degenerate singlet pair against correlations in the many-body state is demonstrated as well as the breaking of the degeneracy by the lowering of symmetry of the CGQD. The band-gap renormalization, electron-hole attraction, fine structure, oscillator strength, and polarization of the exciton are analyzed as a function of the size, shape, screening, and symmetry of the CGQD. The theoretical results are compared with experimental absorption spectra.

DOI: 10.1103/PhysRevB.89.085310 PACS number(s): 81.05.ue, 31.15.aq, 31.15.xr, 71.35.Cc

I. INTRODUCTION

There is currently interest in the optical properties of graphene [1–20] and graphene-based nanostructures, carbon nanotubes [21–31], nanoribbons [32–35], and graphene quantum dots [36–58]. Graphene quantum dots are interesting because their electronic [36–45], magnetic [42,43,46–55], and optical properties [51,55,57,58] can be potentially engineered by controlling their size, shape, edge character, number of layers, and carrier density.

In particular, Li and co-workers described recently a class of colloidal, solution processable graphene quantum dots (CGQDs) with a well defined structure [59–63]. Two classes of dots, with $N = 168$ and 132 atoms, were obtained and the absorption and emission of solutions containing CGQDs were measured [61]. The number of atoms in each dot was determined from mass spectrometry, while the symmetry was inferred through the solution chemistry and infrared vibrational spectra. Since the CGQDs are suspended in solution, whose dielectric constant can be tuned, their optical response can be studied as a function of their size and shape, as well as the strength of the Coulomb interactions. Indeed, optical absorption spectra reveal a clear dependence of the position of the absorption edge on the number of atoms [59–62]. The fluorescence and phosphorescence spectroscopy [61] shows the existence of a gap between emission and absorption spectra interpreted in terms of the energy difference between the singlet and triplet exciton states.

The GCQD with $N = 168$ atoms in vacuum was recently analyzed theoretically by Schumacher [64] using the time-dependent density functional theory (DFT) approach. The numerical simulation revealed the existence of a bright-singlet exciton doublet in a band of dark-triplet and singlet states.

Here we present a microscopic theory of the optical properties of colloidal graphene quantum dots based on a combination of the tight-binding (TB) description of the p_z single-electron states and screened electron-electron interactions treated by exact diagonalization methods in the space of multipair excitations out of the Hartree-Fock (HF) ground state. We find the semiconducting, Mott-insulator, and spin-polarized HF ground states as a function of the strength of the Coulomb interaction. In the semiconductor phase we describe a universal form of the exciton spectrum, with the two bright-singlet exciton states and a band of two dark-singlet and 12 triplet exciton states at low energy, in agreement with the results of Schumacher. We determine the bright-singlet dark-triplet exciton splitting and relate the degeneracy of the bright exciton states to the symmetry of the quantum dot. The effect of the reduction of size and the removal of symmetry on the exciton spectrum is investigated by comparing the $N = 168$ and 132 CGQDs. The theoretical absorption spectra are compared with experiment.

The paper is organized as follows. In Sec. II we describe the structure, model Hamiltonian, and the TB-HF-configuration interaction (CI) method. In Sec. III we present a symmetry analysis of the band-edge exciton spectra of the triangular $N = 168$ CGQD and numerical results for $N = 168$ and 132 CGQDs. In Sec. IV we discuss the effect of screening on optical properties and compare theoretical absorption spectra with the experimental data. Section V contains conclusions.

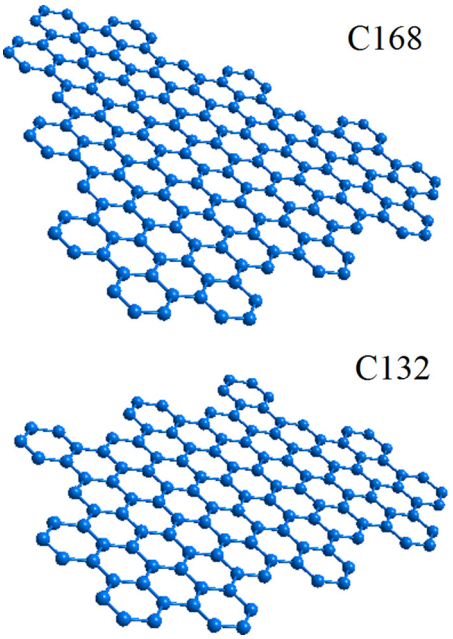

FIG. 1. (Color online) Graphene quantum dots with 132 and 168 atoms. C168 exhibits all point symmetries of the graphene sheet.

II. THE MODEL

The CGQDs C132 and C168 [59–63] are modeled as two-dimensional clusters of carbon atoms, depicted as blue circles, forming the perfect honeycomb lattice with the bond length $a_0 = 0.142$ nm, as shown in Fig. 1. As seen in the figure, the $N = 132$ atom graphene quantum dot is obtained by cutting out the upper corner consisting of 36 carbon atoms from the dot with $N = 168$ atoms. The $N = 132$ CGQD is smaller and does not have the rotational symmetry of the C168 molecule. For both structures, we assume hydrogen passivation and no edge reconstruction [53].

Building on our earlier work [44,52,53,58], we assume that the mobile electrons occupy the states of the π band composed of the spin-degenerate p_z orbitals, one per atom. As a result, the charge-neutral CGQD with N atoms carries N electrons.

We start by describing the motion of a single electron in a lattice of positively charged ions. Out of six electrons belonging to each carbon atom, five are strongly bound, forming the bonds in the plane of the CGQD and partially shielding the Coulomb potential of the carbon nucleus. We expand the wave function in the basis of orthogonalized atomic p_z orbitals $|i\rangle$ localized on atom i. The screened electron-ion interaction $\sum_k V_k$ due to positive ions centered at the kth atom leads to the scattering matrix element $\langle i|\sum_k V_k|j\rangle$ from orbital $|i\rangle$ to $|j\rangle$. Defining the tunneling matrix element as a two-body contribution $t_{ij} = \langle i|(V_i + V_j)|j\rangle$, we are left with three-body contributions $\langle i|\sum_{k\neq i,j} V_k|j\rangle$. In order to compute the three-body terms, we approximate the screened electron-ion interactions V_k by the electron-electron Coulomb elements $\langle i|V_k|j\rangle = -\langle ik|V|kj\rangle$.

Finally, denoting the electron creation operators for state i by $c^+_{i\sigma}$ allows us to write the Hamiltonian for N carbon atoms and N electrons as

$$\hat{H} = \sum_{i,l=1}^{N}\sum_{\sigma}\left[t_{il} - \sum_{k\neq i,l}\langle ik|V|kl\rangle\right]c^+_{i\sigma}c_{l\sigma} + \frac{1}{2}\sum_{i,j,k,l}\sum_{\sigma,\sigma'}\langle ij|V|kl\rangle c^+_{i\sigma}c^+_{j\sigma'}c_{k\sigma'}c_{l\sigma}. \quad (1)$$

In the expression above, the first term is the one-electron Hamiltonian, which describes the interaction between an electron and the shielded ions. It is important to note that the positive charge scattering term depends on the atomic index and is different for the edge and interior atoms of the CGQD. In the following calculations we restrict the tunneling matrix t_{il} to nearest-neighbor (NN), t, and next-nearest-neighbor (NNN), t_2, tunneling. The last term in Eq. (1) describes the screened electron-electron interactions, with the Coulomb matrix element $\langle ij|V|kl\rangle$ defined in the atomic p_z basis $\psi_i(\mathbf{r})$as

$$\langle ij|V|kl\rangle = \iint d\mathbf{r_1}d\mathbf{r_2}\psi^*_i(\mathbf{r_1})\psi^*_j(\mathbf{r_2}) \times \frac{e^2}{\kappa|\mathbf{r_2}-\mathbf{r_1}|}\psi_k(\mathbf{r_2})\psi_l(\mathbf{r_1}). \quad (2)$$

For the full HF treatment, all direct, exchange, and scattering Coulomb matrix elements are computed numerically by approximating the p_z orbitals with Slater functions for up to second-nearest-neighbor atoms [44,52,53,58] while for atoms at greater distances, the matrix elements are approximated by matrix elements corresponding to classical point-charge interactions. Coulomb interactions are assumed to be screened by the effective dielectric constant κ with contributions from both the σ electrons of graphene and the solvent in which the dots are suspended. The Hamiltonian contains two energy scales, the hopping matrix element t and the Coulomb interactions screened by the effective dielectric constant κ. The two energy scales determine the electronic properties of CGQDs.

A. Hartree-Fock approximation

The full interacting Hamiltonian for the N-atom CGQD with $N \sim 10^2$ cannot be diagonalized exactly. Thus we start by solving the Hartree-Fock problem first and treating the interactions among HF quasiparticles second. The HF Hamiltonian is obtained from the full Hamiltonian by replacing the two-body scattering terms with the single-particle scattering from the potential of the mean-field density matrix, which becomes

$$H_{\mathrm{MF}} = \sum_{i,l,\sigma}^{N}\tau_{il}c^+_{i\sigma}c_{l\sigma} + \sum_{i,l,\sigma}^{N}\Bigg[\sum_{j,k,\sigma'}(\langle ij|V|kl\rangle - \langle ij|V|lk\rangle\delta_{\sigma\sigma'})\langle c^+_{j\sigma'}c_{k\sigma'}\rangle\Bigg]c^+_{i\sigma}c_{l\sigma}, \quad (3)$$

where we introduced the effective hopping element $\tau_{il} = t_{il} - \sum_{k\neq i,l}\langle ik|V|kl\rangle$ and $\langle c^+_{j\sigma'}c_{k\sigma'}\rangle = \rho_{jk\sigma'}$ are the elements of the density matrix. The HF operators are defined as linear combinations of atomic operators $b^+_{p\sigma} = \sum_{i=1}^{N} B_{p\sigma,i}c^+_{i\sigma}$ that diagonalize the converged HF Hamiltonian as $H_{\mathrm{MF}} =$

$\sum_{p=1}^{N}\sum_{\sigma}\epsilon_{p\sigma}b^{+}_{p\sigma}b_{p\sigma}$. The HF energies are composed of two parts: $\epsilon_{p\sigma}=E_{p\sigma}+\Sigma(p\sigma)$. The single-particle part, $E_{p\sigma}$, originates from the single-particle tight-binding part of the Hamiltonian $H_{\rm MF}$, and the self-energy, $\Sigma(p\sigma)=\sum_{q=1}^{N_{\rm valence}}(2\langle pq|V_{\rm HF}|qp\rangle-\langle pq|V_{\rm HF}|pq\rangle)$, accounts for all direct and exchange interactions of the electron in the HF orbital p with all other electrons filling the valence band. Note that in the above equation the Coulomb elements in the basis of HF orbitals are obtained by rotating the elements $\langle ij|V|kl\rangle$ defined in the basis of localized orbitals [Eq. (2)]:

$$\langle pq|V_{\rm HF}|rs\rangle=\sum_{i,j,k,l}B_{p,i}B_{q,j}B^{*}_{r,k}B^{*}_{s,l}\langle ij|V|kl\rangle. \quad (4)$$

One can further simplify the problem from the full HF approximation and treat the system in the Hubbard U approximation. Then, instead of using the full Hamiltonian, one would eliminate all Coulomb interactions except for the on-site $U_i=\langle ii|V|ii\rangle$ terms and create Hubbard U quasiparticles.

B. Interaction of HF quasiparticles

The rotation of the single-particle basis, defined by the HF procedure, diagonalizes the mean-field Hamiltonian $H_{\rm MF}$ [Eq. (3)], but not the full Hamiltonian given in Eq. (1). To proceed further, we now rotate the full Hamiltonian into the HF basis. Expressing the operators $c^{+}_{i\sigma}$ ($c_{i\sigma}$) in Eq. (1) in terms of the HF creation (annihilation) operators $b^{+}_{p\sigma}$ ($b_{p\sigma}$) as

$$c^{+}_{i\sigma}=\sum_{p=1}^{N}B^{*}_{p\sigma,i}b^{+}_{p\sigma}, \quad (5)$$

and rewriting the hopping elements τ_{il} in terms of the HF energy levels using Eq. (3), we obtain the full Hamiltonian in the basis of the HF quasiparticles in the form

$$H_{\rm QD}=\sum_{p,q}^{N}\sum_{\sigma}\left(\epsilon_{p\sigma}\delta_{pq}-V^{\rm MF}_{pq\sigma}\right)b^{+}_{p\sigma}b_{q\sigma}+\frac{1}{2}\sum_{p,q,r,s,\sigma,\sigma'}^{N}\langle pq|V_{\rm HF}|rs\rangle b^{+}_{p\sigma}b^{+}_{q\sigma'}b_{r\sigma'}b_{s\sigma}, \quad (6)$$

where

$$V^{\rm MF}_{pq\sigma}=\sum_{r}n_{r,\sigma'}(\langle pr|V_{\rm HF}|rq\rangle-\delta_{\sigma\sigma'}\langle pr|V_{\rm HF}|qr\rangle). \quad (7)$$

Here $n_{r,\sigma'}$ is the number operator determining the occupation of the HF level r by a spin-σ' electron.

C. Correlations via multipair excitations from the HF state

We now proceed to include electronic correlations as interactions of HF quasiparticles using the CI method. The configuration-interaction step involves creating a basis set, including the HF state $|{\rm HF_{gs}}\rangle$ and all the excitations up to the selected number of quasiparticles, constructing the matrix of the Hamiltonian $H_{\rm QD}$ [Eq. (6)] in this basis, and diagonalizing this matrix numerically. As a result, one obtains correlated eigenstates Φ_ν of the form

$$|\Phi_\nu\rangle=k_0|{\rm HF_{gs}}\rangle+\sum_{i,j,\sigma}k^{\nu(1)}_{ij}|i\sigma;j\sigma\rangle+\sum_{i,j,k,l}\sum_{\sigma_1,\sigma_2}k^{\nu(2)}_{ijkl}|i\sigma_1,j\sigma_2;k\sigma_1,l\sigma_2\rangle+\cdots. \quad (8)$$

Here $|p\sigma;q\sigma\rangle=b^{+}_{p\sigma}b_{q\sigma}|{\rm HF_{gs}}\rangle$ are the single-pair excitations that create an electron-hole pair at states p-q, conserving the total projection of the spin. Similarly, $|p\sigma_1,q\sigma_2;r\sigma_1,s\sigma_2\rangle=b^{+}_{p\sigma_1}b^{+}_{q\sigma_2}b_{r\sigma_1}b_{s\sigma_2}|{\rm HF_{gs}}\rangle$ are the two-pair excitations and so on.

In particular, the HF ground state itself is corrected by contributions from multipair excitations. The corrected ground state will then be expressed as Φ_0.

D. Absorption spectra

The absorption spectrum of a photon with energy ω is obtained from Fermi's golden rule:

$$A(\omega)=\sum_{\nu,\nu'}W_\nu|\langle\Phi_{\nu'}|\hat{P}^{+}|\Phi_\nu\rangle|^2\delta(E_{\nu'}-E_\nu-\omega), \quad (9)$$

where E_ν,$E_{\nu'}$ are the energies of the initial and the final state participating in the absorption, $\hat{P}^{+}=\sum_{p,q,\sigma}d(p,q)b^{+}_{p\sigma}b_{q\sigma}$ is the polarization operator adding a pair excitation while annihilating a photon, and W_ν is the probability that the initial many-body state ν is occupied.

We will now elaborate on the dipole element $d(p,q)$ appearing in the polarization operator, which is described in terms of atomic orbitals as

$$d(p,q)=\sum_{i=1}^{N}\sum_{j=1}^{N}B^{*}_{p,i}B_{q,j}\langle i|\vec{\varepsilon}\cdot\vec{r}|j\rangle, \quad (10)$$

where $\vec{\varepsilon}$ is the polarization of light. We first need to evaluate the dipole element in the basis of atomic p_z orbitals. Using the orthogonality of the orbitals, and setting all terms to zero except for the on-site and the NN terms, we get the dipole element between p_z orbitals as [58,65]

$$\langle i|\vec{\varepsilon}\cdot\vec{r}|j\rangle=D_{ij}\vec{\varepsilon}\cdot(\hat{R}_j-\hat{R}_i)(1-\delta_{ij})+\vec{\varepsilon}\cdot\hat{R}_i\delta_{ij}, \quad (11)$$

where the coefficient $D_{ij}=|\int d\vec{r}\phi^{*}_z(\vec{r})\vec{r}\phi_z(\vec{r}-\vec{R}_{\langle ij\rangle})|$ is computed using the Slater p_z orbitals. In our calculations, we include NN and NNN elements which are calculated as $D^{\rm NN}=0.3433$ and $D^{\rm NNN}=0.0873$ in units of nearest neighbor distance, respectively.

III. ELECTRONIC AND OPTICAL PROPERTIES OF $N=168$ COLLOIDAL GRAPHENE QUANTUM DOT

In this section, we apply the TB-HF-CI methodology to the electronic states and absorption spectrum of $N=168$ CGQD.

A. Rotational symmetry

The triangular $N=168$ CGQD is rotationally symmetric and exhibits all point symmetries of the graphene sheet. The three symmetry axes, shown in red, divide the CGQD into three segments, A, B, and C, with 56 atoms each. We assign atomic index j_β ($\beta=A$) to atoms in segment A. Equivalent atoms in

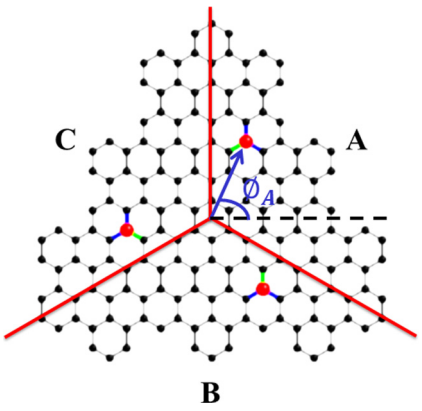

FIG. 2. (Color online) Graphene quantum dot with 168 atoms exhibiting all point symmetries of the graphene sheet. The three symmetry axes are shown in red.

segments B and C, related by a rotation of $\pm\alpha = 2\pi/3$, are shown in Fig. 2.

To proceed further we assign values to atomic segments (A,B,C) as $\{0,1,2\}$. Next, by rotating each atomic orbital group (j_A, j_B, j_C), we construct new basis vectors

$$\Psi_j^m = \frac{1}{\sqrt{3}}(|j_0\rangle + e^{i(m\cdot 2\pi/3)\cdot 1}|j_1\rangle + e^{i(m\cdot 2\pi/3)\cdot 2}|j_2\rangle), \quad (12)$$

with $m = \{0,1,2\}$.

After rotating to the new basis, we find the TB Hamiltonian block diagonal for each $m = \{0,1,2\}$ subspace and, upon diagonalization of the TB Hamiltonian, obtain the single-particle energy levels with eigenvalue index ν and quantum number m, shown in Fig. 3(a). We find the conduction band minimum (CM) and valence band maximum (VM) of the C168 molecule to be degenerate due to the degeneracy of the $m = 1$ and $m = 2$ subspaces, which is a result of the fact that $e^{i2\pi/3} = (e^{i4\pi/3})^* = (e^{-i2\pi/3})^*$. The degeneracy of these levels can be linked to the valley degeneracy of graphene.

We now relate the triangular symmetry to the dipole elements and optical selection rules. Expanding the rotationally invariant eigenvectors $|\nu,m\rangle$ in terms of localized orbitals, Eq. (12), and assuming circular polarization of light $\epsilon_\pm$, after lengthy algebra, we find that the dipole elements between the CM/VM levels satisfy the selection rule

$$\langle\nu',m'|\vec{\varepsilon}\cdot\vec{r}|\nu,m\rangle = \delta_{m',m\pm1}C_{m,m',\nu,\nu'}, \quad (13)$$

where C is a constant determined numerically.

Arrows in Fig. 3(a) show the optical transitions with a finite matrix element while Fig. 3(b) shows all possible transition energies along with their dipole strength between the highest (lowest) three VB (CB) states. We see indeed that the selection rule $\delta_{m',m\pm1}$ is satisfied and all vertical transitions $\Delta m = 0$ are dark. The transitions with $\Delta m = \pm1$ correspond to circularly polarized light with $\sigma = \pm1$ polarizations, in analogy to semiconductor quantum dots. Figure 3(b) shows the dipole matrix elements as a function of transition energy. The lowest-energy transitions between the two top valence and bottom conduction band states correspond to two dipole-active and two dark transitions. The lowest-energy shell is separated by a gap from the next shell. However, the lack of dipole

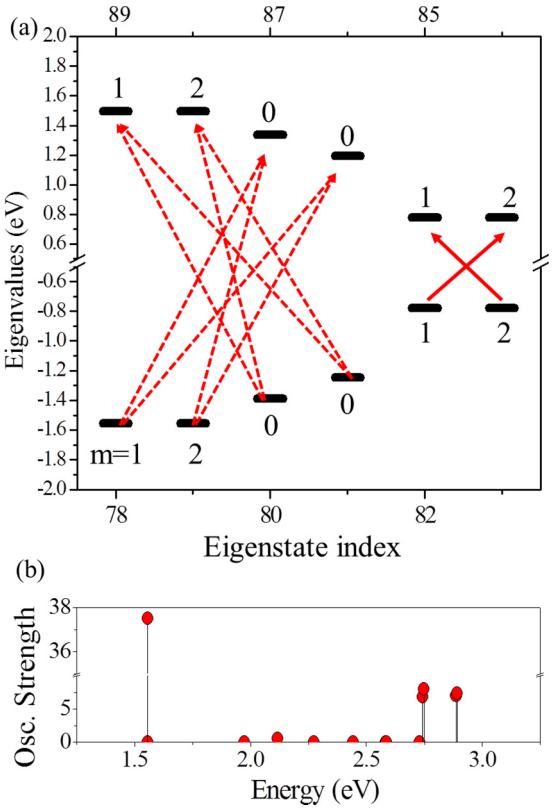

FIG. 3. (Color online) (a) The tight-binding energy levels for C168 for $t = -3.0$ eV, $t_2 = -0.1$ eV, and $\kappa = 5$. Only a few levels around the Fermi level are shown. Dashed lines between CB and VB levels indicate a weak oscillator strength while the solid line corresponds to strong transitions. (b) Oscillator strengths of transitions within the window of 6CB and 6VB levels. The strongest line around 1.5 eV corresponds to a transition between the degenerate CBM and VBM levels, while the second set of transitions at around 2.75 and 2.9 eV is due to transitions between the higher lying $m = 0$ and $m = 1,2$ levels.

moments for some of the transitions between the higher lying $m = \{1,2\}$ states with the $m = 0$ levels visible in Fig. 3(b) is due to the weak overlap of the wave functions and is unrelated to the symmetry.

Below we will analyze the structure of the lowest-energy shell in absorption in the interacting CGQD.

B. Band-edge exciton

Let us now describe the characteristic spectrum of band-edge excitons on the lowest-energy shell. We relabel the two topmost valence band states as $\{v1,v2\}$ and two lowest-energy conduction band states as $\{c1,c2\}$.

We start by filling up all the VB TB orbitals with spin-up and spin-down electrons and forming the HF ground state $|\mathrm{HF_{gs}}\rangle$ as shown in Fig. 4(a). Next, the excitations $|p,q\rangle = b^+_{p\uparrow}b_{q\uparrow}|\mathrm{HF_{gs}}\rangle$ are created. The $\Delta m = \pm1$ optically active excitations are shown in Fig. 4(b). There is only one electron-hole pair with $\Delta m = +1$ and one with $\Delta m = -1$ for a given spin of an excited electron. The energy of each pair, $E_{p,q} = \epsilon_p - \epsilon_q + \Sigma(p) - \Sigma(q) - \langle pq|V_{\mathrm{HF}}|qp\rangle$, is given by a difference

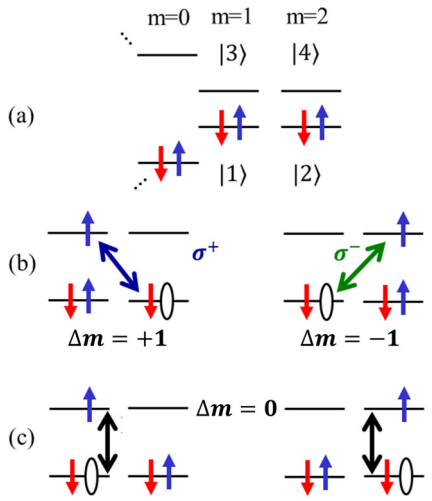

FIG. 4. (Color online) (a) The HF ground state $|\mathrm{HF_{gs}}\rangle$. (b) Single-pair excitation with total angular momentum $\Delta m = +1$ and $\Delta m = -1$. (c) Single-pair excitations from $|\mathrm{HF_{gs}}\rangle$ with total angular momentum $\Delta m = 0$.

in single-particle energies and self-energies Σ between the electron and hole and by the electron-hole attraction.

With two possible $\Delta m = \pm 1$ states and two possible spin directions, there are four exciton states, as shown on the right-hand side of Fig. 5(a). There is one singlet and one triplet state with $S_z = 0$ for each $\Delta m = \pm 1$ state given as $|p,q,S/T\rangle = \frac{(b^+_{p\uparrow} b_{q\uparrow} \pm b^+_{p\downarrow} b_{q\downarrow})}{\sqrt{2}} |\mathrm{HF_{gs}}\rangle$. The energy of the singlet and triplet, $E_{p,q,S/T} = \epsilon_p - \epsilon_q + \Sigma(p) - \Sigma(q) - \langle pq|V_{\mathrm{HF}}|qp\rangle + \langle pq|V_{\mathrm{HF}}|pq\rangle \pm \langle pq|V_{\mathrm{HF}}|pq\rangle$, differs by twice the exchange, which pushes the singlets up in energy. A similar analysis is carried out for the two $\Delta m = 0$ [Fig. 4(c)] dark configurations, as shown on the left-hand side of Fig. 5(a). Two $\Delta m = 0$ configurations of each total spin component interact, and thus their energy is renormalized. The final spectrum of the band-edge excitons is shown in the middle column (Full CI) of Fig. 5(a). We find two bright degenerate singlet exciton states and a band of two dark-singlet and four dark-triplet exciton states at lower energies. If we count all possible S_z configurations, the low-energy band consists of two dark-singlet and 12 dark-triplet states. By comparing Fig. 5(a) obtained from full HF quasiparticles and Fig. 5(b) obtained from Hubbard U quasiparticles in the semiconductor regime, we see that the separation of the degenerate bright singlets from the forest of dark singlets and triplets is robust. However, the ordering of the levels in the dark region changes from Hubbard U to full HF due to the inclusion of exchange interactions which drive the lowest excited state from a singlet to a triplet.

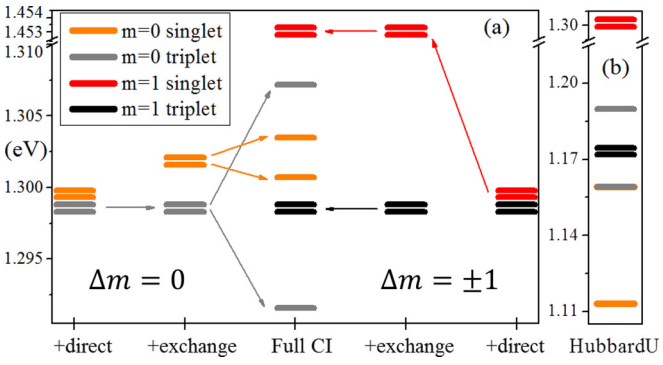

FIG. 5. (Color online) (a) Evolution of singlet-triplet splitting with the inclusion of different interactions in C168 for $t = -3.0$ eV, $t_2 = -0.1$ eV, and $\kappa = 5$ starting with the full HF ground state. The black lines are $\Delta m = \pm 1$ triplets, red are $\Delta m = \pm 1$ singlets, while $\Delta m = 0$ triplet and singlet levels are shown in gray and orange. The left section shows the evolution of $\Delta m = 0$ excitons while the right section shows the evolution of $\Delta m = \pm 1$ excitons. The middle section depicts all Δm levels after full CI calculations. (b) Starting with the Hubbard U ground state, the singlet-triplet splitting after full CI.

C. Numerical results

We now turn to the numerical analysis of the absorption spectrum. We start with a comparison of the TB and fully self-consistent Hartree-Fock energy spectra. Figure 6 shows the tight-binding and fully self-consistent Hartree-Fock energy levels for $\kappa = 5$, $t = -3.0$ eV, and $t_2 = -0.1$ eV, both normalized to the middle of the energy gap. We see that the HF energy spectrum, renormalized by the self-energy, resembles closely the tight-binding spectrum. In particular, the degeneracy of VB maximum (VBM) and CB minimum (CBM) is preserved. The main differences between spectra are the breaking of electron-hole symmetry and changes in the electron bandwidth, which are expected in HF.

By minimizing the energy of the ground state through the self-consistent HF procedure, we obtain the quasiparticle states and energy levels as well as the interactions between HF quasiparticles. Next, we compute the ground and excited states and the absorption spectrum using the TB-HF-CI approach.

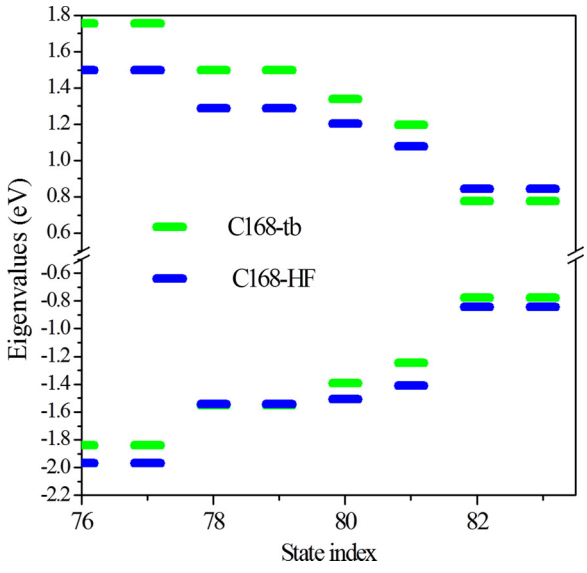

FIG. 6. (Color online) The self-consistent Hartree-Fock and tight-binding energy levels for C168 for $\kappa = 5$, $t = -3.0$ eV, $t_2 = -0.1$ eV. Only a fraction of the levels around the Fermi level are shown.

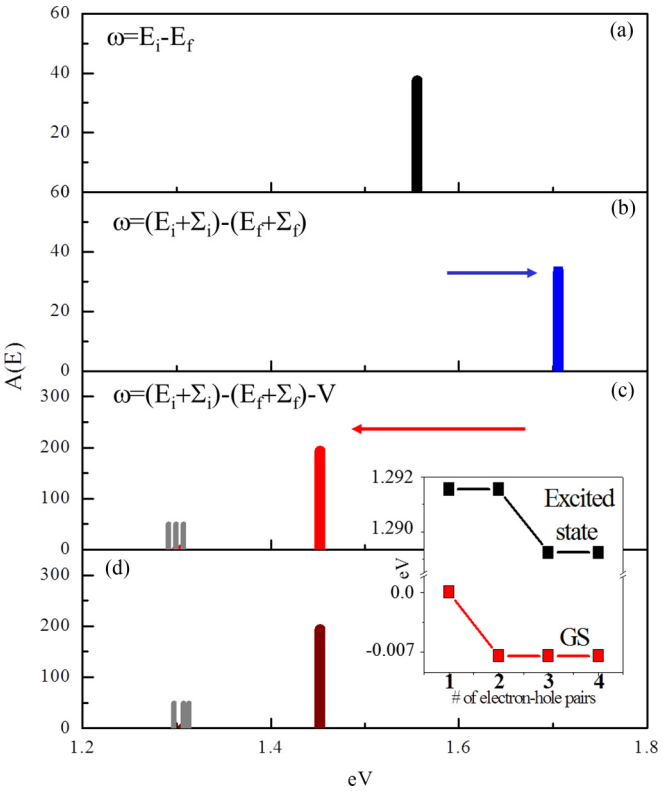

FIG. 7. (Color online) Evolution of absorption spectrum of C168 for $t = -3.0$ eV, $t_2 = -0.1$ eV, and $\kappa = 5.0$, with increasing accuracy of approximations: (a) TB absorption spectrum, (b) blueshift due to self-energy correction, (c) inclusion of electron-hole attraction and correlations, and (d) renormalization of the ground state and exciton spectrum due to interaction with up to four-pair excitations.

This allows us to discuss the robustness of the band-edge excitons and absorption spectrum discussed above.

Figure 7 shows the evolution of the low-energy excitonic spectrum associated with the degenerate VBM/CBM states. The topmost panel shows the absorption spectrum of the noninteracting CGQD. The second panel shows the absorption in the TB-HF approximation. The self-consistent HF approach protects the rotational invariance of the $m = \{0, 1, 2\}$ subspaces but blueshifts the energy gap due to differences in self-energy of the electron and the hole, as expected.

The third panel of Fig. 7 shows the band-edge exciton spectrum calculated from the HF ground state. We see that the inclusion of electron-hole attraction, exchange, and electron-hole correlations redshifts the absorption spectrum and separates in energy the singlet and triplet excitons. The two bright excitons remain degenerate, and a band of dark singlets and triplet exciton states appears at lower energy. The last row in Fig. 7 shows the absorption spectrum calculated using renormalized ground and excited states obtained after the inclusion of all possible configurations with up to four pairs within the limited Hilbert space of four VB and four CB HF states. The renormalization of the energy of the ground and excited triplet states with the number of excited pairs is shown in the inset. We see that the inclusion of multipair excitations renormalizes both the ground state and the excited states, but does not significantly shift the transition energies nor does it remove degeneracies or change the structure of the absorption spectra. We conclude that the absorption spectrum obtained from an exciton excited out of a HF ground state is a good approximation for a semiconductor CGQD. Below we will discuss how the absorption depends on the tunneling matrix element and on screening of electron-electron interactions.

IV. EFFECTS OF SCREENING κ AND TUNNELING t

The ground state properties depend strongly on the values of the strength of screening and the amplitude of the hopping term. Previous work on the ground state properties of graphene [66–69] suggest that for strong Coulomb interactions, or small values of κ, there exists a transition from a semimetallic, weakly interacting phase to a Mott-insulating, strongly correlated phase. Below we discuss the phase diagram of C168 as a function of κ and t. Figure 8(a) shows the energy of the full HF and Hubbard U ground states for the spin-polarized, $S_z = N/2$, and spin-unpolarized, $S_z = 0$, C168 as a function of κ for $t = -4.2$ eV. We see that, compared to the spin-polarized case, the spin-unpolarized phase is the ground state for all κ down to $\kappa = 1.4$ in full HF while the spin-polarized state is predicted as the ground state at $\kappa < 1.4$ using the full HF approximation. Figure 8(b) shows the calculated average density matrix element $\rho_\sigma = \langle c^+_{i\sigma} c_{j\sigma} \rangle$ for i, j nearest neighbors, averaged over all pairs for a spin-unpolarized ground state as a function of κ. The density matrix element shows the probability of having two electrons with the same spin on nearest-neighbor orbitals. For large κ we find $\rho_\sigma = 0.26$, i.e., the value for the HF state of bulk graphene [56]. The local values of ρ_σ of course differ from the bulk value at the edges even at the high-κ range. Using full HF, as κ decreases, we see the onset of the phase transition at around $\kappa < 1.8$. For $\kappa < 1.8$ the ground state departs from the semiconducting state of graphene and becomes a Mott insulator, with spin-up electrons on lattice A and spin-down electrons on lattice B. Increasing the magnitude of the hopping

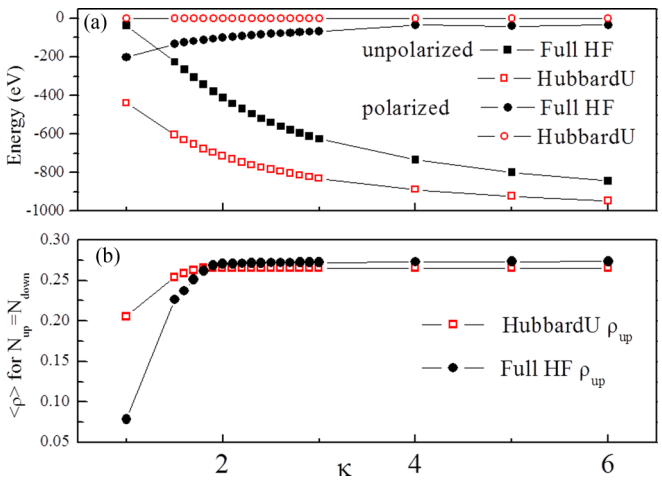

FIG. 8. (Color online) Phase diagram of C168 at $t = -4.2$ eV, $t_2 = -0.1$ eV. (a) Ground state energy of the spin-polarized and spin-unpolarized C168 and (b) the nearest-neighbor up-spin density matrix element of the spin-unpolarized C168 as a function of screening strength κ calculated with Hubbard U and full HF approaches.

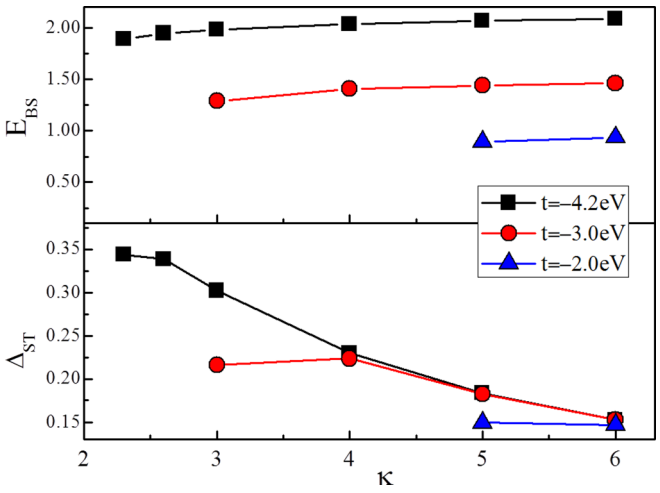

FIG. 9. (Color online) Position of the bright degenerate singlet and the bright-singlet–dark-triplet separation as a function of κ.

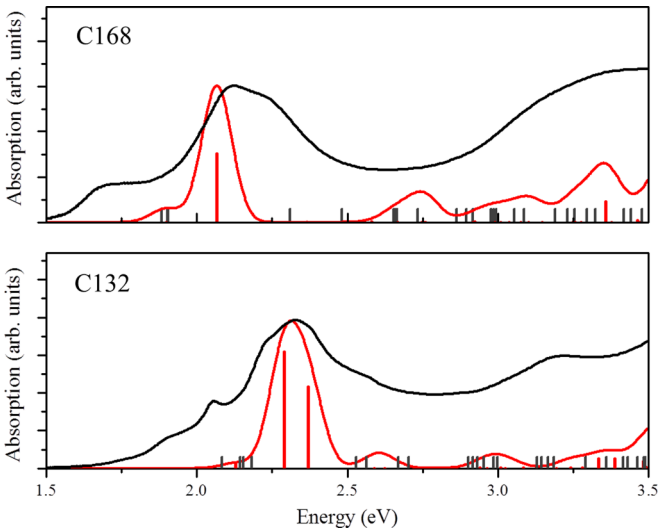

FIG. 10. (Color online) Absorption spectrum of C168 (upper spectrum) and C132 (lower spectrum) compared with the experiment at $t = -4.2$ eV, $t_2 = -0.1$ eV, and $\kappa = 5$. Here, 10% of the highest absorption peak has been assigned to absorption of dark singlets. The red solid line is the calculated absorption. Red drop lines are singlet absorption peaks, gray drop lines represent the location of triplets, and the black solid line is the experimental absorption data.

parameter t results in a phase transition at lower κ values. However, in Hubbard U we do not observe a pronounced spin separation compared to full HF.

We now discuss the evolution of the exciton spectra as a function of t and κ in the semiconducting phase. Figure 9(a) presents the results of the calculated energy of the bright degenerate singlets and $\Delta_{S/T}$ while the separation between the bright singlet and the lowest-energy dark triplet as a function of t and κ is given in Fig. 9(b). We see that the energy of the bright singlets weakly depends on κ but varies with tunneling matrix element t from $\sim$1 eV for $t = -2$ eV to $\sim$2 eV for $t = -4.2$ eV. The bright-singlet–dark-triplet separation $\Delta_{S/T}$ is due to electron-electron interactions and is influenced by the dielectric constant κ rather than the hopping element t. For $t = -4.2$ eV, $\Delta_{S/T}$ varies from 0.15 eV for $\kappa \sim 6$ to 0.35 eV at $\kappa \sim 2$.

We now compare the calculated absorption spectra with experiment. Figure 10(a) shows the measured [61] and calculated absorption spectra for $\kappa = 5.0$ and $t = -4.2$ eV. We have used Gaussian broadening in continuous plots and added 10% of the oscillator strength of the brightest peak to the dark singlets since they may contribute to absorption if the symmetry is broken due to, e.g., charge and spin fluctuations in the surrounding fluid. We see that the measured absorption spectra show an absorption threshold around $E = 1.8$ eV, a peak at $E = 2.25$ eV, and a reduced absorption strength up until $E = 3$ eV. Our preliminary interpretation assigns the peak in the measured absorption spectrum at $E = 2.25$ eV to the bright-singlet excitons while we predict the absorption threshold as due to dark singlets, which dictates the choice of t and κ. The calculated absorption spectrum can reproduce the position of the absorption peak due to bright excitons followed by a gap. However, the singlet-triplet splitting is significantly underestimated when compared with experiment.

A. Effect of reduced size and symmetry: $N = 132$ colloidal graphene quantum dot

We now proceed to discuss the effect of reduced size and symmetry on the optical properties of CGQDs. C132, shown in Fig. 1, can be obtained from C168 by cutting off one corner, and hence it lacks C_3 symmetry. As a result, the degeneracy of the top of the valence band and bottom of the conduction band is removed and there are nonzero dipole elements between all CB and VB levels. The degeneracy of the high-energy bright singlets is removed and the low-energy dark singlets acquire nonzero oscillator strength. Figure 10(b) shows the calculated and measured absorption spectrum for C132. Due to reduced size and increased confinement of Dirac fermions, the C132 absorption spectrum is blueshifted compared to C168, both in experiment and in theory. The calculated spectra show the splitting of the bright-singlet exciton peak. The splitting is not visible in experiments on ensembles of CGQDs in a fluid. Again, the singlet-triplet splitting is underestimated compared to experiment.

V. CONCLUSIONS

We presented a microscopic theory of electronic and optical properties of colloidal graphene quantum dots (CGQDs) based on the tight-binding, Hartree-Fock, and configuration interaction approaches. The low-energy exciton spectrum is predicted to consist of two bright-singlet exciton states corresponding to two circular polarizations of light and a lower-energy band of two dark singlets and 12 dark triplets. The effects of symmetry, size, shape, screening, band-gap renormalization, electron-hole correlations, and many-body corrections are analyzed. The theoretical results are compared with experimental absorption spectra. While a good overall agreement is found, the singlet-triplet splitting is underestimated. Future theoretical work should improve on the screening of the Coulomb interaction and the effects of lattice vibrations on the absorption and emission spectra. Future

experimental work should attempt to identify the degenerate singlet states in C168 and their splitting in C132 colloidal graphene quantum dots.

ACKNOWLEDGMENTS

I.O. and P.H. thank NSERC and Canadian Institute for Advanced Research for support.

[1] P. R. Wallace, Phys. Rev. **71**, 622 (1947).
[2] K. S. Novoselov, A. K. Geim, S. V. Morozov, D. Jiang, Y. Zhang, S. V. Dubonos, I. V. Grigorieva, and A. A. Firsov, Science **306**, 666 (2004).
[3] K. S. Novoselov, A. K. Geim, S. V. Morozov, D. Jiang, M. I. Katsnelson, I. V. Grigorieva, S. V. Dubonos, and A. A. Firsov, Nature (London) **438**, 197 (2005).
[4] Y. B. Zhang, Y. W. Tan, H. L. Stormer, and P. Kim, Nature (London) **438**, 201 (2005).
[5] S. Y. Zhou, G. H. Gweon, J. Graf, A. V. Fedorov, C. D. Spataru, R. D. Diehl, Y. Kopelevich, D. H. Lee, S. G. Louie, and A. Lanzara, Nat. Phys. **2**, 595 (2006).
[6] A. H. Castro Neto, F. Guinea, N. M. R. Peres, K. S. Novoselov, and A. K. Geim, Rev. Mod. Phys. **81**, 109 (2009).
[7] A. K. Geim and K. S. Novoselov, Nat. Mater. **6**, 183 (2007).
[8] A. K. Geim, Science **324**, 1530 (2009).
[9] C. Faugeras, M. Amado, P. Kossacki, M. Orlita, M. Kühne, A. A. L. Nicolet, Yu. I. Latyshev, and M. Potemski, Phys. Rev. Lett. **107**, 036807 (2011).
[10] D. M. Hoffman, P. C. Eklund, R. E. Heinz, P. Hawrylak, and K. R. Subbaswamy, Phys. Rev. B **31**, 3973 (1985).
[11] J. Blinowski, N. H. Hau, C. Rigaux, J. P. Vieren, R. Le Toullec, G. Furdin, A. Herold, and J. Melin, J. Phys. (Paris) **41**, 47 (1980).
[12] M. L. Sadowski, G. Martinez, M. Potemski, C. Berger, and W. A. de Heer, Phys. Rev. Lett. **97**, 266405 (2006).
[13] M. Orlita, C. Faugeras, P. Plochocka, P. Neugebauer, G. Martinez, D. K. Maude, A. L. Barra, M. Sprinkle, C. Berger, W. A. de Heer, and M. Potemski, Phys. Rev. Lett. **101**, 267601 (2008).
[14] R. R. Nair, P. Blake, A. N. Grigorenko, K. S. Novoselov, T. J. Booth, T. Stauber, N. M. R. Peres, and A. K. Geim, Science **320**, 1308 (2008).
[15] F. Wang, Y. B. Zhang, C. S. Tian, C. Girit, A. Zettl, M. Crommie, and Y. R. Shen, Science **320**, 206 (2008).
[16] Z. Q. Li, E. A. Henriksen, Z. Jiang, Z. Hao, M. C. Martin, P. Kim, H. L. Stormer, and D. N. Basov, Nat. Phys. **4**, 532 (2008).
[17] K. F. Mak, M. Y. Sfeir, Y. Wu, C. H. Lui, J. A. Misewich, and T. F. Heinz, Phys. Rev. Lett. **101**, 196405 (2008).
[18] M. Koshino and T. Ando, Phys. Rev. B **77**, 115313 (2008).
[19] T. Mueller, F. N. A. Xia, and P. Avouris, Nat. Photonics **4**, 297 (2010).
[20] L. Yang, J. Deslippe, C. H. Park, M. L. Cohen, and S. G. Louie, Phys. Rev. Lett. **103**, 186802 (2009).
[21] F. Wang, G. Dukovic, L. E. Brus, and T. F. Heinz, Science **308**, 838 (2005).
[22] M. Y. Sfeir, T. Beetz, F. Wang, L. Huang, X. M. H. Huang, M. Huang, J. Hone, S. O'Brien, J. A. Misewich, T. F. Heinz, L. Wu, Y. Zhu, and L. E. Brus, Science **312**, 554 (2006).
[23] J. Lefebvre and P. Finnie, Phys. Rev. Lett. **98**, 167406 (2007).
[24] R. Matsunaga, K. Matsuda, and Y. Kanemitsu, Phys. Rev. Lett. **106**, 037404 (2011).
[25] T. Ando, J. Phys. Soc. Jpn. **74**, 777 (2005).
[26] S. Uryu and T. Ando, Phys. Rev. B **74**, 155411 (2006).
[27] C. L. Kane and E. J. Mele, Phys. Rev. Lett. **93**, 197402 (2004).
[28] E. J. Mele and C. L. Kane, Solid State Commun. **135**, 527 (2005).
[29] Z. Wang, H. Zhao, and S. Mazumdar, Phys. Rev. B **74**, 195406 (2006).
[30] V. Perebeinos, J. Tersoff, and P. Avouris, Phys. Rev. Lett. **92**, 257402 (2004).
[31] C. D. Spataru, S. Ismail-Beigi, R. B. Capaz, and S. G. Louie, Phys. Rev. Lett. **95**, 247402 (2005).
[32] Y.-W. Son, M. L. Cohen, and S. G. Louie, Phys. Rev. Lett. **97**, 216803 (2006).
[33] J. Alfonsi and M. Meneghetti, New J. Phys. **14**, 053047 (2012).
[34] M. Y. Han, B. Ozyilmaz, Y. Zhang, and P. Kim, Phys. Rev. Lett. **98**, 206805 (2007).
[35] X. Li, X. Wang, L. Zhang, S. Lee, and H. Dai, Science **319**, 1229 (2008).
[36] J. S. Bunch, Y. Yaish, M. Brink, K. Bolotin, and P. L. McEuen, Nano Lett. **5**, 287 (2005).
[37] T. Ihn, S. Gustavsson, U. Gasser, B. Kung, T. Muller, R. Schleser, M. Sigrist, I. Shorubalko, R. Leturcq, and K. Ensslin, Solid State Commun. **149**, 1419 (2009).
[38] L. A. Ponomarenko, F. Schedin, M. I. Katsnelson, R. Yang, E. W. Hill, K. S. Novoselov, and A. K. Geim, Science **320**, 356 (2008).
[39] B. Wunsch, T. Stauber, and F. Guinea, Phys. Rev. B **77**, 035316 (2008).
[40] J. Wurm, A. Rycerz, I. Adagideli, M. Wimmer, K. Richter, and H. U. Baranger, Phys. Rev. Lett. **102**, 056806 (2009).
[41] F. Libisch, C. Stampfer, and J. Burgdorfer, Phys. Rev. B **79**, 115423 (2009).
[42] J. Akola, H. P. Heiskanen, and M. Manninen, Phys. Rev. B **77**, 193410 (2008).
[43] M. Ezawa, Phys. Rev. B **81**, 201402 (2010).
[44] P. Potasz, A. D. Guclu, and P. Hawrylak, Phys. Rev. B **81**, 033403 (2010).
[45] P. Potasz, A. D. Guclu, and P. Hawrylak, Phys. Rev. B **82**, 075425 (2010).
[46] L. C. Campos, V. R. Manfrinato, J. D. Sanchez-Yamagishi, J. Kong, and P. Jarillo-Herrero, Nano Lett. **9**, 2600 (2009).
[47] M. Ezawa, Phys. Rev. B **76**, 245415 (2007).
[48] J. Fernandez-Rossier and J. J. Palacios, Phys. Rev. Lett. **99**, 177204 (2007).
[49] W. L. Wang, S. Meng, and E. Kaxiras, Nano Lett. **8**, 241 (2008).
[50] J. Jung and A. H. MacDonald, Phys. Rev. B **79**, 235433 (2009).
[51] T. Yamamoto, T. Noguchi, and K. Watanabe, Phys. Rev. B **74**, 121409 (2006).
[52] A. D. Guclu, P. Potasz, O. Voznyy, M. Korkusinski, and P. Hawrylak, Phys. Rev. Lett. **103**, 246805 (2009).
[53] O. Voznyy, A. D. Guclu, P. Potasz, and P. Hawrylak, Phys. Rev. B **83**, 165417 (2011).
[54] P. Potasz, A. D. Guclu, O. Voznyy, J. A. Folk, and P. Hawrylak, Phys. Rev. B **83**, 174441 (2011).

[55] A. D. Guclu and P. Hawrylak, Phys. Rev. B **87**, 035425 (2013).
[56] P. Potasz, A. D. Guclu, A. Wojs, and P. Hawrylak, Phys. Rev. B **85**, 075431 (2012).
[57] Z. Z. Zhang, K. Chang, and F. M. Peeters, Phys. Rev. B **77**, 235411 (2008).
[58] A. D. Guclu, P. Potasz, and P. Hawrylak, Phys. Rev. B **82**, 155445 (2010).
[59] X. Yan, X. Cui, and L. Li, J. Am. Chem. Soc. **132**, 5944 (2010).
[60] X. Yan, X. Cui, B. Li, and L. Li, Nano Lett. **10**, 1869 (2010).
[61] M. L. Mueller, X. Yan, J. A. McGuire, and L. Li, Nano Lett. **10**, 2679 (2010).
[62] X. Yan, B. Li, X. Cui, Q. Wei, K. Tajima, and L. Li, J. Phys. Chem. Lett. **2**, 1119 (2011).
[63] X. Yan, B. Li, and L. Li, Acc. Chem. Res. **46**, 2254 (2013).
[64] S. Schumacher, Phys. Rev. B **83**, 081417 (2011).
[65] M. Zielinski, M. Korkusinski, and P. Hawrylak, Phys. Rev. B **81**, 085301 (2010).
[66] S. Sorella and E. Tosatti, Europhys. Lett. **19**, 699 (1992).
[67] T. O. Wehling, E. Sasioglu, C. Friedrich, A. I. Lichtenstein, M. I. Katsnelson, and S. Blügel, Phys. Rev. Lett. **106**, 236805 (2011).
[68] S. Sorella, Y. Otsuka, and S. Yunoki, Sci. Rep. **2**, 992 (2012).
[69] A. H. MacDonald, J. Jung, and F. Zhang, Phys. Scr., **T 146**, 014012 (2012).